CHEMISTRY OF MATERIALS
Article

Chem. Mater. **2010,** *22,* 893–897 893
DOI:10.1021/cm901682y

Oxygen Transport in Sc-Doped CeO_2: Cation (^{45}Sc) NMR as a Probe of Anionic Conductivity†

Hugo J. Avila-Paredes,‡ Pragati Jain, Sabyasachi Sen, and Sangtae Kim*

Department of Chemical Engineering and Materials Science, University of California, Davis, California 95616

Received June 17, 2009. Revised Manuscript Received August 11, 2009

Oxygen-vacancy hopping dynamics in Sc-doped CeO_2, a solid electrolyte (SE), was studied employing high-temperature (up to 600 °C) ^{45}Sc nuclear magnetic resonance (NMR) and electrochemical impedance spectroscopy (EIS) techniques. The oxygen-vacancy hopping frequency and its temperature dependence, as obtained from the simulation of ^{45}Sc NMR line shapes, are in excellent agreement with those obtained from EIS. The characteristic length scale of the vacancy hopping is found to be controlled by the average Sc−Sc separation in the lattice. Moreover, direct spectroscopic evidence for the presence of small but significant dynamical heterogeneities is observed, implying that all vacancies are not characterized by similar dynamic properties. These results clearly demonstrate that cation NMR can serve as a unique probe for anionic transport in SEs.

1. Introduction

The ever-growing interest in the transport properties of solid electrolytes (SEs) such as fluorite-structured doped ZrO_2 and CeO_2 reside in their applications, for instance, in solid oxide fuel cells and oxygen sensors.[1−6] Oxygen-ion conduction in these materials involves thermally activated hopping of these ions through the crystal lattice at a rate that depends primarily on the concentration, distribution, and mobility of oxygen vacancies in the atomic structure. Despite a good understanding of the general principles of oxygen-ion conduction, a lack of information about atomic-scale oxygen-ion hopping dynamics in these SEs has hindered full development of fundamental predictive models of their properties. The information regarding the ionic dynamics in these materials primarily comes from electrical conductivity measurements. However, such measurements reveal information on the average mobility of the ions undergoing long-range diffusion in the system with little direct microstructural understanding of the conduction mechanisms. The temperature dependence of NMR line shape and of nuclear spin−lattice relaxation (SLR) time have been demonstrated to be powerful tools for studying the atomic-scale mechanisms and time scales of various dynamical phenomena including atomic hopping and molecular rotation in solids and liquids.[7−11] Most of the previous NMR studies of oxygen dynamics in SEs have been limited to the application of ^{17}O SLR time (T_1) measurements in doped ZrO_2 and CeO_2.[12−17] Such measurements are typically sensitive to high-frequency dynamics in the tens to hundreds of MHz frequency range, which are often in the range of ion-hopping frequencies in conductive solids at high temperatures. Although such data yield information on the time scale and activation energy (E_a) of dynamics responsible for SLR, it is difficult in practice to relate such data to the atomic-scale mechanistic details of ionic motion without theoretical modeling. On the other hand, high-resolution and high-temperature ^{17}O magic-angle-spinning (MAS) NMR line shape simulation can yield direct site-specific information on dynamics and the associated atomic-scale mechanism in SEs. Such studies have only become possible relatively recently with the availability of high-temperature MAS NMR probes.[12,13,15] However, the results of these studies on doped ZrO_2 and CeO_2 have exhibited large discrepancies between the time scale as well as E_a of the fundamental

† Accepted as part of the 2010 "Materials Chemistry of Energy Conversion Special Issue".

‡ Current address: Departamento de Ingeniería de Procesos e Hidráulica, Area de Ingeniería Química, Universidad Autónoma Metropolitana, Unidad Iztapalapa, Av. San Rafael Atlixco 186, Col. Vicentina, Mexico city, 09340, Mexico.

*Corresponding author. E-mail: chmkim@ucdavis.edu.

(1) Tuller, H. L.; Nowick, A. S. *Solid State Sci. Technol.* **1975**, *122*, 255–259.
(2) Singhal, S. C. *Solid State Ionics* **2000**, *135*, 305–313.
(3) Skinner, S. J.; Kilner, J. A. *Mater. Today* **2003**, *6*, 30–37.
(4) Minh, N. Q. *J. Am. Ceram. Soc.* **1993**, *76*, 563–588.
(5) Winter, M.; Brodd, R. J. *Chem. Rev.* **2004**, *104*, 4245–4270.
(6) Steele, B. C. H. *High Conductivity Solid Ionic Conductors, Recent Trends and Applications*; World Scientific: London, U.K., 1989, p. 402.
(7) Farnan, I.; Stebbins, J. F. *Science* **1994**, *265*, 1206–1209.
(8) Stebbins, J. F.; Xu, Z.; Vollath, D. *Solid State Ionics* **1995**, *78*, L1–L8.
(9) Sen, S.; Stebbins, J. F. *Phys. Rev. Lett.* **1997**, *78*, 3495–3498.
(10) León, C.; Santamaría, J.; París, M. A.; Sanz, J.; Ibarra, J.; Várez, A. *J. Non Cryst. Solids* **1998**, *235−237*, 753–760.
(11) Stebbins, J. F. *Science* **2002**, *297*, 1285–1286.
(12) Viefhaus, T.; Bolse, T.; Müller, K. *Solid State Ionics* **2006**, *177*, 3063–3068.
(13) Kim, N.; Hsieh, C.-H.; Huang, H.; Prinz, F. B.; Stebbins, J. F. *Solid State Ionics* **2007**, *178*, 1499–1506.
(14) Huang, H.; Hsieh, C.-H.; Kim, N.; Stebbins, J. F.; Prinz, F. *Solid State Ionics* **2008**, *179*, 1442–1445.
(15) Kim, N.; Stebbins, J. F. *Chem. Mater.* **2007**, *19*, 5742–5747.
(16) Fuda, K.; Kishio, K.; Yamauchi, S.; Fueki, K. *J. Phys. Chem. Sol.* **1985**, *46*, 1141.
(17) Adler, S. B.; Reimer, J. A. *Solid State Ionics* **1996**, *91*, 175.

Published on Web 09/04/2009

oxygen-vacancy hopping process and that of ionic conductivity. A number of possible reasons have been put forward to explain such discrepancies including the possibility that ^{17}O NMR line shape is sensitive to local, backward-forward correlated jumps that do not contribute to long-range diffusion and conductivity.[13]

Recent studies have shown the potential of high-resolution ^{89}Y and ^{45}Sc MAS NMR spectroscopic techniques for direct quantitative characterization of dopant cation coordination environments with zero, one and two oxygen vacancies in Y and Sc-doped ZrO_2 and CeO_2.[18,19] Hopping of oxygen-ions/vacancies in and out of the first coordination shell of Y^{3+} or Sc^{3+} at high temperatures should consequently be detectable as a "virtual" chemical exchange between these cation sites that are coordinated to 6, 7, or 8 oxygens or equivalently to 2, 1, and 0 oxygen vacancies (denoted henceforth as $X^{[6]}$, $X^{[7]}$, and $X^{[8]}$, respectively with X = Y or Sc). Moreover, cross-exchange between $X^{[6]}$, $X^{[7]}$, and $X^{[8]}$ sites would require long-range transport of oxygen vacancies from one dopant cation site to another. We have carried out a combined ^{45}Sc MAS NMR and EIS study of the oxygen-vacancy hopping dynamics in a 5 cat. % Sc doped CeO_2 (SDC) sample over a wide range of temperatures in order to verify these hypotheses. We report here the results of this study that provide important and unique site-specific information regarding long-range oxygen-ion/vacancy dynamics in the SE, and demonstrate that cation NMR can serve as a probe for anionic conductivity of SEs.

2. Experimental Section

The initial powder of SDC was synthesized via a precipitation method using NH_4OH(aq) as precipitating agent and nitrates of the cations as precursors. Details of the synthesis can be found elsewhere.[19] The powder was calcined at 700 °C for 2 h under air, prior to the consolidation into cylindrical pellets via cold isostatic pressing at 276 MPa. The green pellets were sintered at 1400 °C for 5 h, with heating and cooling rates of 5 °C/min, under air. The density of the pellets determined by an Archimedes method was 94% of the theoretical density of ceria.

For NMR measurements, a sintered pellet was ground in an agate mortar. The desired fluorite cubic crystal structure of the obtained powder was verified with X-ray diffraction (Scintag XDS-2000) and its particle size (~200 nm) was determined from field-emission scanning electron microscopy (SEM) images (microscope FEI XL30-SFEG). The dopant content of the samples, analyzed using energy dispersive X-ray spectroscopy in an SEM (microscope FEI XL30-SFEG operated at 10 kV of accelerating voltage), was 5.3 ± 0.6 cat. % Sc. ^{45}Sc MAS NMR spectra were collected at a Larmor frequency of 121.49 MHz (11.7 T) using a Bruker wide-bore magnet and a Bruker Avance-500 solid state NMR spectrometer. ^{45}Sc MAS NMR spectra were collected at room temperature and below (down to −80 °C) collected using a Bruker 4 mm triple resonance probe. The SDC powder was loaded into a 4 mm ZrO_2 rotor and a spectra were collected using a $\pi/24$ rf pulse (0.12 μs) and a recycle delay of 0.2 s at a spinning speed of 10 kHz. Approximately 20,000 scans were averaged and Fourier-transformed to obtain each of these ^{45}Sc MAS NMR spectrum. The high-temperature ^{45}Sc MAS NMR spectra of Sc-doped CeO_2 were collected using a high-temperature MAS probe (Doty Inc.). The powdered sample was loaded into a boron nitride capsule that was inserted into a 7 mm Si_3N_4 rotor and was spun at spinning rates of between 3.5 and 4.5 kHz. N_2 gas boil off from a high-pressure liquid nitrogen dewar was used for spin and temperature control of the sample. The temperature of the probe was calibrated externally using the well-known temperature dependence of the ^{207}Pb chemical shift of $Pb(NO_3)_2$, before and after the ^{45}Sc NMR measurements.[20] The sample temperature was raised from 25 to 600 °C stepwise in 50 °C increments and allowed to reach equilibrium at each temperature for 15 min before data collection. All high-temperature ^{45}Sc MAS NMR spectra were collected using a $\pi/2$ rf pulse (1 μs) and a recycle delay of 0.2 s. Approximately 2000 to 6000 FIDs were averaged and Fourier-transformed to obtain each ^{45}Sc MAS NMR spectrum. The ^{45}Sc NMR chemical shifts were externally referenced to an aqueous solution of $ScCl_3$ ($\delta_{iso} = 0$ ppm).

For impedance measurements, two parallel faces of a sintered pellet were polished and painted with Pt paste (5349 Heraeous). To ensure good contact of the electrodes (Pt) with the sample, the pellet was annealed at 1000 °C for 5 h, with heating and cooling rates of 5 °C/min, under air. The impedance measurements of the SDC pellet were carried out under air in the temperature range of 250−700 °C, using a Novocontrol Alpha−AN modulus analyzer in the frequency range of 1×10^{-1} to 1×10^{-7} Hz. The fittings of the measured impedance spectra with an appropriate equivalent circuit model (see below for details) were performed using the software Z-View.

3. Results and Discussion

Figure 1 shows the ^{45}Sc MAS NMR spectra of the SDC powder collected at temperatures ranging from −80 °C up to 600 °C. At room temperature and below, these spectra exhibit two sharp and well-resolved resonances at ~23 and −34 ppm that can be assigned to $Sc^{[7]}$ and $Sc^{[8]}$ sites, respectively.[19] Integration of the peak areas indicates that these two Sc sites are present at a ratio of ~60:40. Because replacement of every pair of Ce atoms in the CeO_2 lattice with a pair of Sc atoms results in the formation of one oxygen vacancy, this result implies that all the oxygen vacancies in the lattice of this SDC sample are associated with Sc atoms as nearest neighbors. As the temperature increases, the two peaks in the ^{45}Sc MAS NMR spectrum become broader but still remain distinguishable up to 300 °C. These two resonances also become deshielded (move to higher parts per million values) at constant rates of 0.03 and 0.05 ppm/°C in this temperature range. This deshielding must result from the thermal expansion of the lattice that affects the chemical shifts of the two Sc sites slightly differently. The ^{45}Sc MAS NMR spectrum at 300 °C also shows the presence of a broad peak centered at the weighted average of the positions of the two principal peaks, implying fast dynamical cross-exchange between a small subpopulation of

(18) Sen, S.; Avila-Paredes, H. J.; Kim, S. *J. Mater. Chem.* **2008**, *18*, 3915.
(19) Jain, P.; Avila-Paredes, H. J.; Gapuz, C.; Sen, S.; Kim, S. J. Phys. Chem. C **2009**, ASAP.
(20) Takahashi, T.; Kawashima, H.; Sugisawa, H.; Baba, T. *Solid State Nucl. Magn. Reson.* **1999**, *15*, 119.

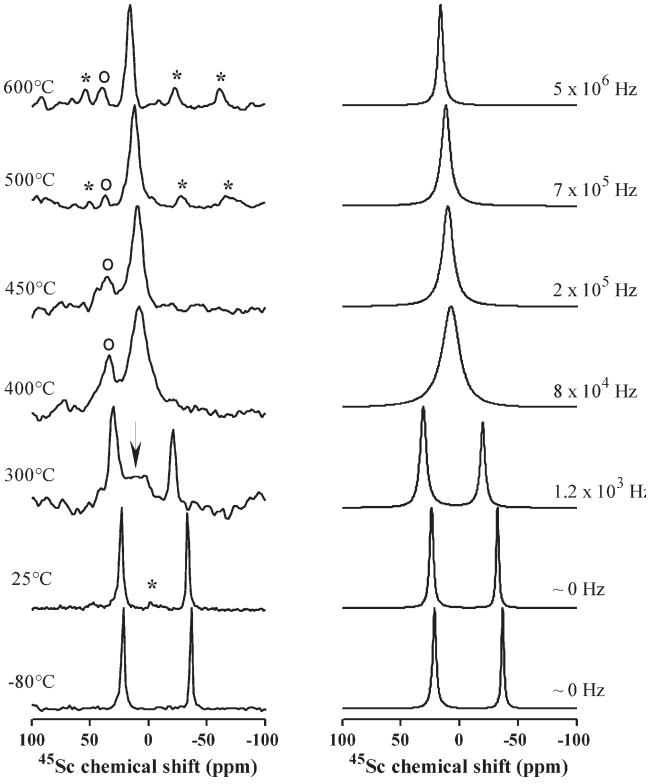

Figure 1. Experimental (left) and simulated (right) ^{45}Sc MAS NMR spectra of SDC. Temperatures and corresponding exchange frequencies are indicated alongside each spectrum. Asterisks correspond to spinning sidebands. Circles correspond to signals from unexchanged $Sc^{[7]}$ sites. The arrow shows a fast-exchanging subpopulation (~20%) of $Sc^{[7]}$ and $Sc^{[8]}$ sites at 300 °C.

the $Sc^{[7]}$ and $Sc^{[8]}$ sites that results into coalescence of the peaks. Further increase in temperature results in complete coalescence of the two Sc peaks into a single broad peak. The width of this dynamically averaged peak decreases monotonically with increasing temperature and is indicative of increasing cross-exchange frequency between the two Sc sites. This peak is always located at the weighted average of the positions of $Sc^{[7]}$ and $Sc^{[8]}$ peaks and shifts also at a weighted average rate of 0.04 ppm/°C in the temperature range between 400 and 600 °C (Figure 1). This result suggests that the relative fractions of $Sc^{[7]}$ and $Sc^{[8]}$ sites in the lattice are independent of temperature at least up to 600 °C. The diffusion coefficient of Sc^{3+} ions in this temperature range is expected to be negligibly small and hence can not be responsible for the observed dynamical cross-exchange between the $Sc^{[7]}$ and $Sc^{[8]}$ sites. Instead, the cross-exchange must result from the dynamical transformation between $Sc^{[8]}$ and $Sc^{[7]}$ sites when an oxygen vacancy hops into (out of) the coordination sphere of a $Sc^{[7]}$ ($Sc^{[8]}$) site. These processes can be represented in the form of a transformation reaction: $Sc^{[8]} + V_O^{\bullet\bullet} \leftrightarrow Sc^{[7]}$ where $V_O^{\bullet\bullet}$ represents an oxygen vacancy in the Koger−Vink notation.

The high-temperature ^{45}Sc MAS NMR line shapes were simulated using a standard two-site random cross-exchange model in order to obtain the exchange frequency between $Sc^{[7]}$ and $Sc^{[8]}$ sites in the lattice as a function of temperature (cf. Figure 1). The analytic expression for the line shape resulting from cross-exchange between N distinct sites is given by the real part of $g(\omega)$ given as[21]

$$g(\omega) = \frac{1}{N}\frac{L}{(1 - L/\tau_{NMR})} \quad (1)$$

where

$$L = \sum_{j=1,N} [i(\omega - \omega_j) + 1/T_{2j} + N/\tau_{NMR}]^{-1}$$

where ω_j is the frequency and T_{2j} is the reciprocal of the intrinsic line width corresponding to the site j, N is equal to 2, and $1/\tau_{NMR}$ is the frequency of exchange or dynamical transformation between the two Sc sites. The value of T_{2j} has been kept constant at 0.6 ms for both Sc sites in all of the simulations. A single average temperature-dependent exchange frequency ${\tau_{NMR}}^{-1}$ is found to be sufficient for simulation of all spectra except for the one at 300 °C that required a small subpopulation (~20%) of fast-exchanging Sc sites with hopping frequency of $\sim 1 \times 10^4$ Hz in addition to the slow-exchanging majority of Sc atoms that are hopping at a rate of $\sim 1 \times 10^3$ Hz (Figure 1). On the other hand, the ^{45}Sc MAS NMR spectra in the temperature range between 400 and 600 °C contain an unexchanged $Sc^{[7]}$ signal that indicates the presence of a small population of vacancies (~ 9% of total Sc at 600 °C) that do not participate in the hopping process even at such relatively high temperature. These results imply the presence of small but significant dynamical heterogeneities in the system and provide direct experimental evidence that all vacancies are indeed not the same in their dynamical properties. This issue will be discussed further in detail in a forthcoming paper.

The frequency dependent ac conductivity $\sigma(\omega)$ of SDC is computed over a wide range of frequency, ω, using the values of the real and imaginary parts of the impedance, $Z'(\omega)$ and $Z''(\omega)$, respectively, as obtained from EIS measurements and using the relation

$$\sigma(\omega) = \sqrt{Z'(\omega)^2 + Z''(\omega)^2}\left(\frac{L}{A}\right) \quad (2)$$

where L and A denote the sample thickness and the electrode area, respectively. The $\sigma(\omega)$ of SDC presents two distinctive regions over the frequency range of interest as seen in Figure 2 that can be described by the Almond−West expression[22]

$$\sigma(\omega) = \sigma_{dc}\{1 + (\omega/\omega_h)^n\} \quad (3)$$

where σ_{dc} and ω_h denote the bulk dc-conductivity and the average hopping frequency of oxygen vacancies, respectively, and n is a fitting parameter. This expression implies

(21) Mehring, M. *Principles of High Resolution NMR in Solids*; Springer-Verlag: Berlin, 1983.
(22) Almond, D. P.; Duncan, G. K.; West, A. R. *Solid State Ionics* **1983**, *8*, 159–164.

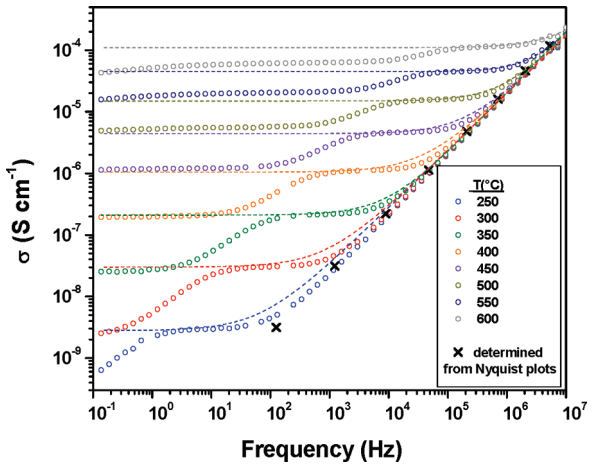

Figure 2. Bode plot displaying frequency dependence of $\sigma(\omega)$of a SDC sample at different temperatures. Open circles correspond to experimental data measured by EIS and dotted lines are the best fits obtained using the Almond−West expression (see text for details).

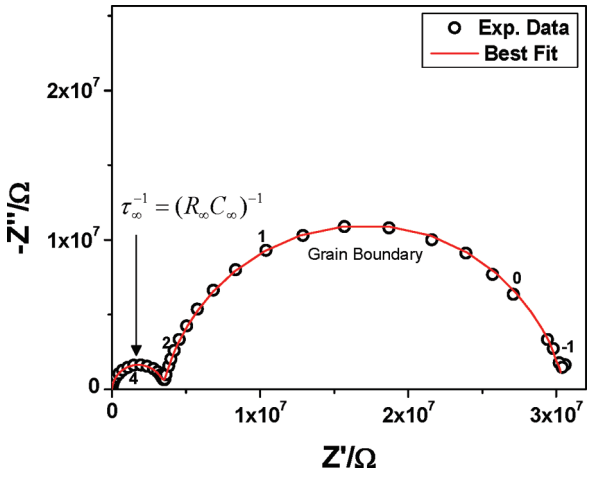

Figure 3. Representative impedance spectrum (a Nyquist plot) of a 5 cat. % Sc-doped ceria sample measured at 350 °C under air. The smaller semicircular arc corresponds to the bulk, owing to the fact that the dielectric constant estimated from C_∞ is consistent with the bulk dielectric constant of CeO_2 (~30). The solid-line indicates the best fit using an equivalent circuit (see the text for details).

that $\sigma(\omega) = \sigma_{dc}$ when $\omega \ll \omega_h$, while $\sigma(\omega) = \sigma_{dc}(\omega/\omega_h)^n$ if $\omega \gg \omega_h$. The $\sigma(\omega)$data at various temperatures have been fitted to this expression to determine the temperature dependence of σ_{dc} and ω_h in SDC. The $\sigma(\omega)$ measured at temperatures above 300 °C shows an additional plateau at lower frequencies (Figure 2), representing the grain-boundary dc-conductivity which will not be discussed further in this paper. It may be noted that ω_h is expected to be identical to the conductivity relaxation frequency τ_∞^{-1} in the bulk (where $\tau_\infty = R_\infty C_\infty$ with R_∞ and C_∞ being the resistance and the capacitance of the bulk, respectively) which corresponds to the frequency at which $-Z''(\omega)$ reaches a maximum when plotted against $Z'(\omega)$ (i.e., a Nyquist plot, Figure 3) and therefore can be directly computed from R_∞ and C_∞ estimated from the best fit of the plot using an equivalent circuit consisting of two parallel RC elements in series corresponding to the bulk and the grain boundary.

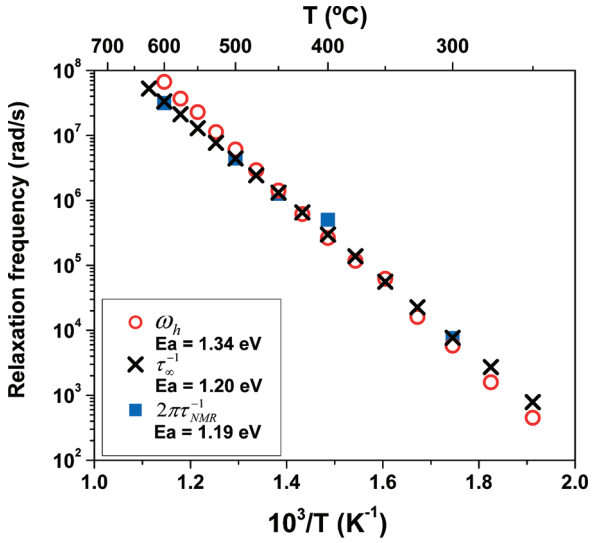

Figure 4. Arrhenius plots of the bulk conductivity relaxation frequencies (circles and crosses) determined from EIS results and oxygen-vacancy hopping frequencies determined from simulation of ^{45}Sc MAS NMR line shapes (squares).

Figure 4 presents an Arrhenius plot of the temperature dependence of the "virtual" exchange frequency between $Sc^{[7]}$ and $Sc^{[8]}$ sites τ_{NMR}^{-1} and of ω_h and τ_∞^{-1} determined from EIS measurements. As expected, the values of ω_h and τ_∞^{-1} are consistent with each other (Figure 4). The activation energies (E_a) of ω_h and τ_∞^{-1} are found to be ~1.34 and 1.20 eV, respectively. This difference in E_a can be attributed to the small discrepancy between ω_h and τ_∞^{-1} resulting from the fitting errors associated with the estimation of ω_h as indicated in Figure 2. It is worth mentioning that these E_a values are also in excellent agreement with that of σ_{dc} (~1.24 eV, not shown here) determined from Figure 2. This is not so surprising because C_∞ often depends on temperature rather weakly such that the measured E_a of τ_∞^{-1} should be close to that of R_∞ which is identical to E_a of σ_{dc}. More importantly, the τ_∞^{-1} values appear to be in excellent agreement with τ_{NMR}^{-1} values over the entire temperature range with an E_a of ~1.19 eV (Figure 3).

It is remarkable that information about oxygen-vacancy dynamics can be successfully obtained by probing the cross-exchange rate between cation coordination environments at elevated temperatures. Clearly, the oxygen vacancy hopping between the coordination spheres of two $Sc^{[7]}$ sites (i.e., a self-exchange) does not lead to the cross-exchange process $Sc^{[8]} + V_O^{\bullet\bullet} \leftrightarrow Sc^{[7]}$ observed here. Similarly, vacancy hopping within the coordination sphere of a $Sc^{[7]}$ site itself may not result in cross-exchange, unless $Sc^{[7]}$ and $Sc^{[8]}$ sites exist as next-nearest neighbors. The latter scenario of clustering of Sc^{3+} ions is highly unlikely considering the relatively small concentration of Sc in the sample studied here. Hence, the average rate of cross-exchange rate between the $Sc^{[7]}$ and $Sc^{[8]}$ sites should correspond to the effective rate of oxygen-vacancy transport across the coordination spheres of dissimilar Sc environments (i.e., $Sc^{[7]}$ and $Sc^{[8]}$). This transport process must involve oxygen-vacancy

hopping in the coordination spheres of Ce ions in the intervening region of the lattice between pairs of $Sc^{[7]}$ and $Sc^{[8]}$ sites because the typical separation distances between such pairs of sites in the structure would be too large (~10 Å) for a single direct hop to take place. If this hypothesis is correct, then the effective oxygen-vacancy hopping distance responsible for cross-exchange between should correspond well with the average separation distance between pairs of $Sc^{[7]}$ and $Sc^{[8]}$ sites in the SDC lattice. The latter is estimated to be ~11 Å for a random distribution of 5 cat % Sc with nearly equal proportions of $Sc^{[7]}$ and $Sc^{[8]}$ sites and a measured density of ~7.02 g cm^{-3} for the sample. On the other hand, for the other extreme scenario where vacancies are always shared between a pair of $Sc^{[7]}$ sites, the average separation distance between pairs of $Sc^{[7]}$ and $Sc^{[8]}$ sites, assuming there is no spatial correlation between these two types of sites, would be ~13 Å. The effective oxygen-vacancy hopping distance d can be computed from τ_{NMR}^{-1} (or τ_{∞}^{-1}) and σ_{dc} using the Nernst−Einstein relation for a random walk model of vacancy diffusion that predicts

$$\sigma_{dc} = \frac{z_i^2 e^2 c_i \gamma d^2 (2\pi\tau_{NMR}^{-1})}{6kT} \quad (4)$$

with z, e, k, and T being charge number, elementary charge, Boltzmann constant and absolute temperature, respectively; γ is a correlation factor that can be approximated to be unity for the small concentration of oxygen vacancies in the sample studied here. This calculation yields a value of $d \approx 14$ Å that corresponds quite well with the average separation distance of ~ 11 to 13 Å between pairs of $Sc^{[7]}$ and $Sc^{[8]}$ sites in the SDC lattice, especially considering all the experimental uncertainties and theoretical approximations involved in estimating these distances. Therefore, when taken together, these results directly indicate that the characteristic length scale associated with ionic conduction in SEs at small carrier concentrations is similar to the average separation distance between dopant cations with and without oxygen vacancies as nearest neighbors and that cation NMR can indeed serve as a unique probe for oxygen-ion transport in SEs.

4. Conclusions

We have estimated oxygen-vacancy hopping frequency and its temperature dependence in 5 cat. % Sc-doped CeO_2 over a wide range of temperatures (−80 to 600 °C) by means of both high-temperature ^{45}Sc MAS NMR and EIS. The absolute values of the hoping frequencies and their activation energies determined from both techniques are in excellent agreement. The effective vacancy hopping distance in this SE determined using the Nernst−Einstein relation was consistent with the average Sc−Sc separation in the lattice, suggesting that characteristic length scale of oxygen transport is in fact governed by the average distance between dopant cations in this material. We have also provided spectroscopic evidence that the oxygen vacancies in this SE exhibit dynamical heterogeneities so that around one tenth of the oxygen vacancies in the material are nearly immobile even at temperatures as high as 600 °C. Our results unambiguously demonstrate that the information about long-range oxygen transport in SEs can be reliably and uniquely obtained at an atomistic level using dopant-cation NMR.

Acknowledgment. H.J.A.P. is grateful to the National Council on Science and Technology of Mexico (CONACYT) and the University of California for the UC-Mexus grant provided for his graduate studies.